Rapid Communications

Contributions of oxygen vacancies and titanium interstitials to band-gap states of reduced titania

Jingfeng Li,* Rémi Lazzari,† Stéphane Chenot,‡ and Jacques Jupille§
CNRS, Sorbonne Universités, UPMC Université Paris 06, UMR 7588, Institut des NanoSciences de Paris, 75005 Paris, France

(Received 2 July 2017; published 9 January 2018)

The spectroscopic fingerprints of the point defects of titanium dioxide remain highly controversial. Seemingly indisputable experiments lead to conflicting conclusions in which oxygen vacancies and titanium interstitials are alternately referred to as the primary origin of the Ti 3*d* band-gap states. We report on experiments performed by electron energy loss spectroscopy whose key is the direct annealing of only the very surface of rutile $TiO_2(110)$ crystals and the simultaneous measurement of its temperature via the Bose-Einstein loss/gain ratio. By surface preparations involving reactions with oxygen and water vapor, in particular, under electron irradiation, vacancy- and interstitial-related band-gap states are singled out. Off-specular measurements reveal that both types of defects contribute to a unique charge distribution that peaks in subsurface layers with a common dispersive behavior.

DOI: 10.1103/PhysRevB.97.041403

Already used in self-cleaning coatings and dye-sensitized solar cells, titanium dioxide TiO_2 offers promising solutions to water/air purification and water splitting [1,2]. Its rich physics and chemistry is mostly tied to the reduced TiO_{2-x} form in which dominant point defects, bridging oxygen vacancies (O_b-vac) and titanium interstitials (Ti_{int}) widely explored on rutile (110) [2–6] (Fig. 1), play a pivotal role. At the origin of the *n*-type electron conductivity, excess electrons generated by defects populate Ti 3*d* related band-gap states (BGS). They have long been associated with O_b-vac (herein labeled V-BGS) because O_2 dissociation both eliminates O_b-vac and heals them by a charge transfer toward O_b and O adatoms (O_{ad}) adsorbed on five-coordinated Ti_{5c} [7]. The model became hotly debated when vacancy-free $TiO_2(110)$ obtained by reacting off H from hydroxylated TiO_{2-x} was shown to retain most of the BGS that were consequently related to Ti_{int} (I-BGS) [4]. Their healing by O_2 was explained by a charge donation from Ti_{int} that promotes a non-vacancy-related O_2 dissociation [4]. Consistently, the TiO_x islands formed upon annealing O-covered rutile [4,8–12] were attributed to the reaction of O_{ad} with Ti_{int} which, as the reoxidation of TiO_{2-x} [13], relies on the diffusion of Ti_{int} in rutile above 400 K. Finally, extra O_{ad} atoms (relative to dissociation on O_b-vac), obtained by reacting O_2 with TiO_{2-x}, were associated with charge transfer from Ti_{int} [4,14]. Additional support given to the O-vacancy model [7] fed the controversy. The oxidative chemistry of TiO_{2-x} was suggested to be controlled by a donor species (O_b-vac and OH) rather than Ti_{int} [15] and, based on a relationship of proportionality between O_b-vac counting by microscopy and photoemission signals, BGS appeared to mostly stem from O_b-vac [16].

The crux of the debate is that the signatures of V-BGS and I-BGS look identical. The case is tackled herein by the rarely used high-resolution electron energy loss spectroscopy (HREELS). The key experiment to single out BGS contributions is the quick annealing (up to 1000 K within a few seconds) of the surface only via a hot filament facing the crystal within the spectrometer, while probing *T* (temperature) via the Bose-Einstein statistics (Fig. S1 in Supplemental Material [18]) of the loss/gain phonon ratio. Annealed samples are labeled SA-*T*-TiO_2 hereafter. Controversial or unexplained data involving annealing treatments, electron bombardment, and exposures to O_2 and H_2O, have been revisited to feature I-BGS and V-BGS. Finally, BGS in-depth profiles [19–23] were probed by off-specular EELS.

$TiO_2(110)$ single crystals were mounted in an ultrahigh vacuum (UHV) setup [24] equipped with an EELS spectrometer (Sec. S1 in Supplemental Material [18]). Sputtering and annealing $TiO_2(110)$ resulted in reduced dark blue color samples R-TiO_2 whose surfaces could be reoxidized (O-TiO_2) by 30 min annealing (1100 K) [9] and cooling in O_2 (5×10^{-6} mbar) at a rate of $\sim$30 K min^{-1} (Sec. S1 in Supplemental Material [18]). EEL spectra were collected between 100 and 300 K. Unless stated, they were recorded in specular geometry (incident angle $\Theta_I = 60^\circ$, incident plane along the $[1\bar{1}0]$ direction) at an energy of $E_I = 38$ eV. Typical EELS spectra (Fig. S3 in Supplemental Material [18]) show broad BGS features at $\sim$0.8 eV before the onset of band-to-band excitations at 3.2 eV. Bulk sensitivity at the phonon energies provides a reliable intensity normalization (Sec. S3 in Supplemental Material [18]). Exposures are expressed in Langmuir (1 L = 1.33×10^{-6} mbar s^{-1}). EELS spectra recorded on R-TiO_2 at 100 K [Fig. S3(a) in Supplemental Material [18]] and 300 K [Fig. S3(b) in Supplemental Material [18]] under O_2 show progressive BGS healing, although the kinetics are different. The fast and slow decreases in BGS intensity that are observed at 100 and 300 K, respectively, rely on mechanisms that are under debate [10,13,25]. Importantly, the similarity between the final BGS intensities [Fig. S3(a) inset in Supplemental Material [18]] indicates two equivalent healing processes.

The preparation of SA-TiO_2 surfaces is central in pinpointing the categories of point defects. Indisputable proof of the existence of I-BGS is provided by the defect peak growing on

*jingfeng.li1987@gmail.com
†Corresponding author: remi.lazzari@insp.jussieu.fr
‡stephane.chenot@insp.jussieu.fr
§jacques.jupille@insp.jussieu.fr

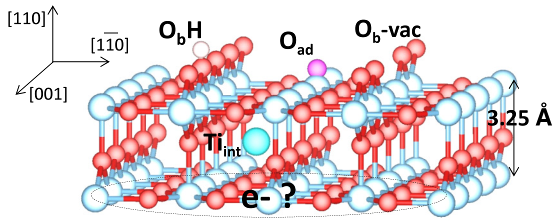

FIG. 1. Ball model of defective $TiO_2(110)$ (Ti, O, H, Ti_{int}, and O_{ad} are blue, red, white, cyan, and pink spheres, respectively); bridging oxygen rows involve O_b-vac and O_bH; O_{ad} lie on Ti_{5c}; Ti_{int} occupy octahedral sites [17]; the localization of excess electrons (question mark) associated with defects is under debate.

SA-420 K-TiO_2 [Fig. 2(a)]. The formation of O_b-vac at 420 K being excluded, this peak is assigned to I-BGS formed via an outward Ti_{int} diffusion [4,26–28] as supported by the square root of the time dependence of the BGS intensity [Fig. 2(a) inset].

In contrast to the slow kinetics of BGS formation on SA-420 K-TiO_2 [Fig. 2(a)], SA-TiO_2 surfaces prepared by annealing of 10 s above 800 K [Fig. 2(b)] show strong BGS whose intensity rises with T. Indeed, O_b-vac are expected to form [3], but it is unclear whether defect states are I-BGS or V-BGS. More is learned of I-BGS by preparing SA-TiO_2 at increasing temperature followed by 20 L of O_2 at 300 K [Fig. 2(c), steps 1–4; inset: BGS intensities]. First, healing I-BGS from SA-420 K-TiO_2 by O_2 (step 1) validates the non-vacancy-related O_2 dissociation associated with charge transfer from Ti_{int} [4,14]. Then, increasing BGS are observed on SA-970 K-TiO_2 and SA-1140 K-TiO_2 although, surprisingly, the residual BGS observed after O_2 exposure continuously decreases through steps 1, 2, and 4 [Fig. 2(c)]. Extra healing of O_b-vac is excluded since there is no reason why reacting O_b-vac with 20 L of O_2 should leave fewer O_b-vac sites intact while their initial concentration is higher. Therefore, Fig. 2(c) shows that the commonly observed residual BGS (Fig. S4 in Supplemental Material [18] and Refs. [4,16,25]) mostly involve I-BGS. Annealing O-covered surfaces at increasing temperature triggers outward Ti_{int} dif-

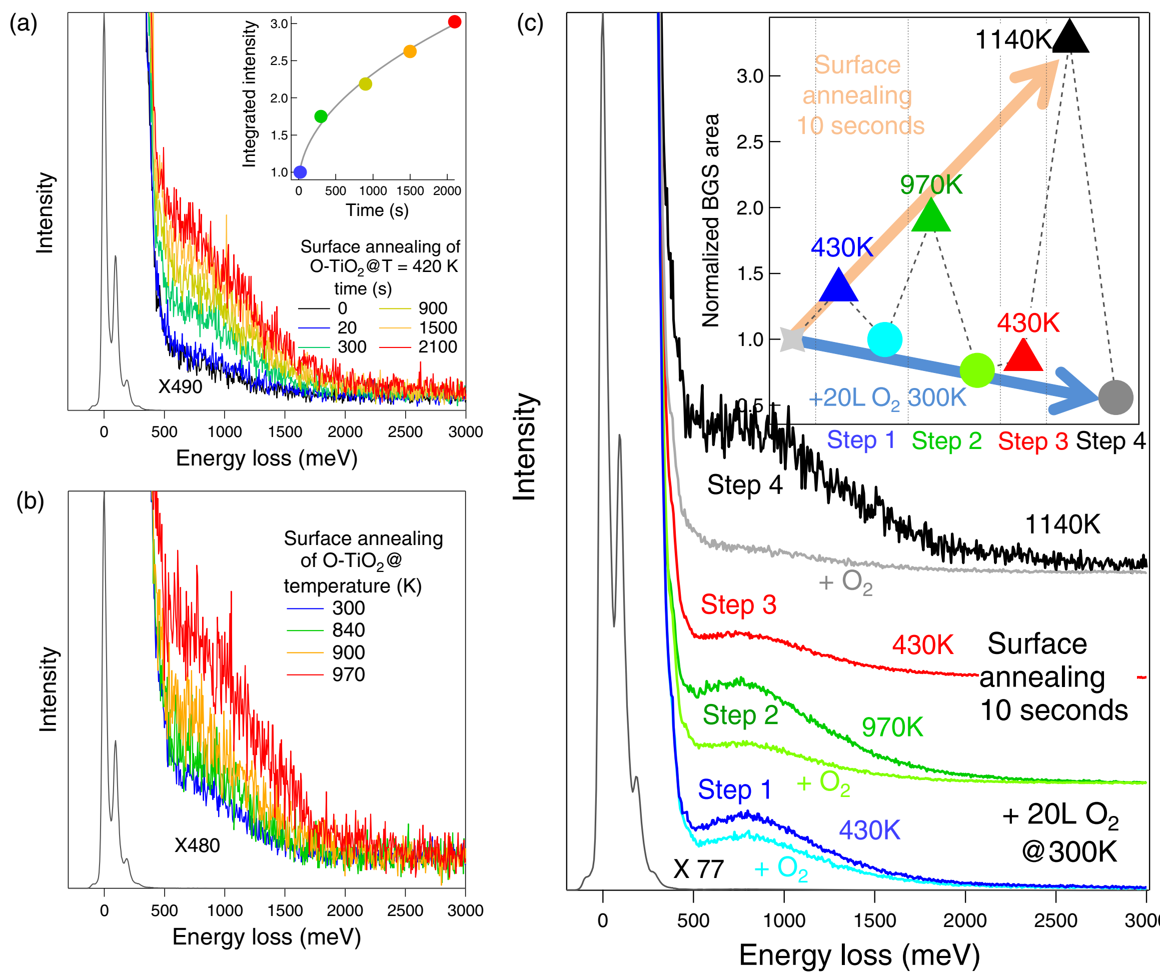

FIG. 2. Singling out BGS from Ti_{int} by surface annealing of O-TiO_2. EELS measurements at 300 K: (a) BGS recorded on SA-420 K-TiO_2 vs time. Inset: Time evolution of the BGS area (500–2500 meV) fitted by a square-root function. (b) BGS from SA-TiO_2 prepared at different temperatures during 10 s. (c) BGS recorded upon successive treatments (steps 1–4): Surface annealing (10 s) at given temperatures (strong color) and then 20 L of O_2 (light color) at 300 K (from bottom to top). Inset: BGS intensities step by step. The black dotted lines show the order of treatments, and the orange and blue arrows to guide the eye evidence an increase in BGS intensity upon an increase in annealing temperature and a corresponding decrease in residual intensity after 20 L O_2.

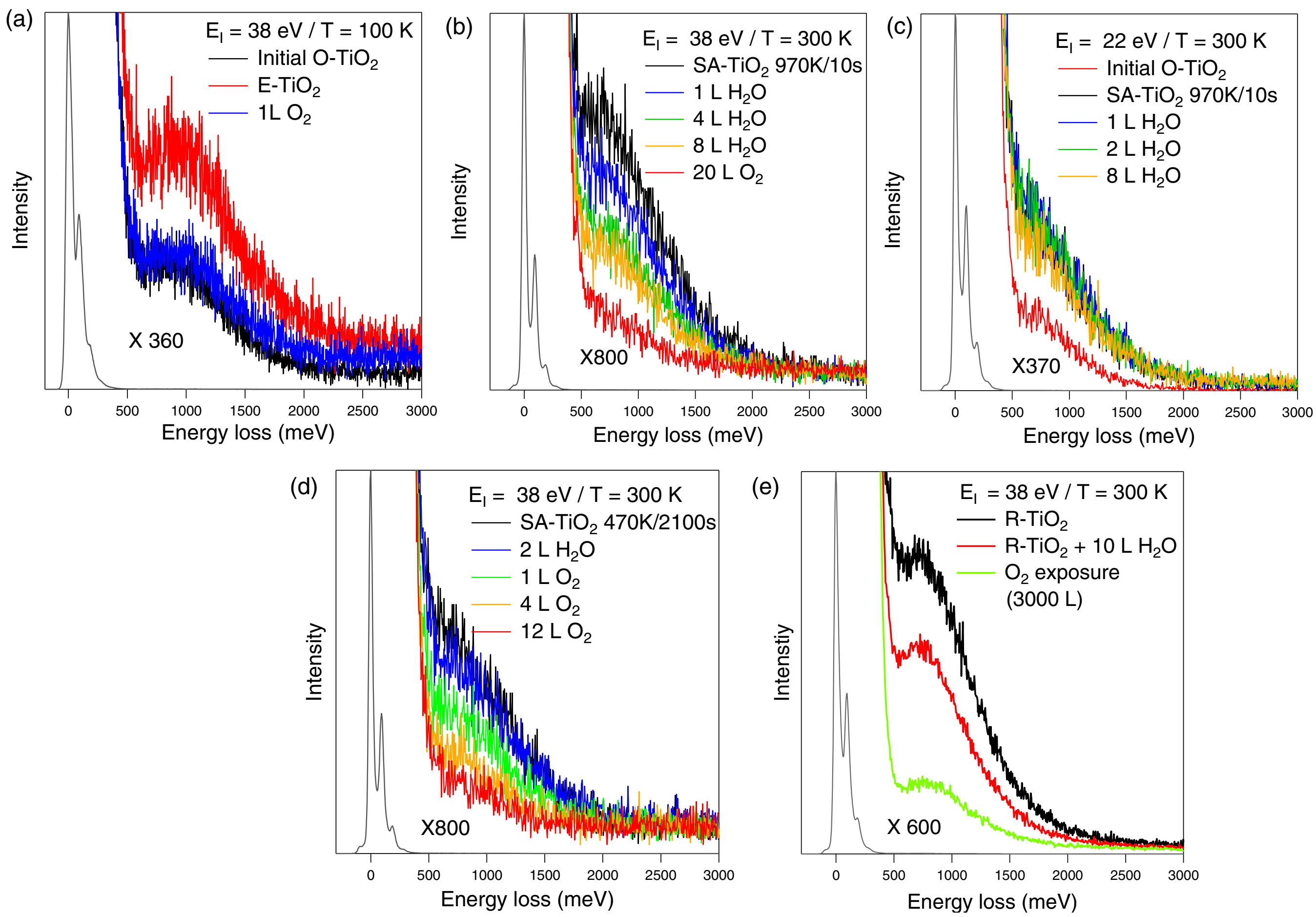

FIG. 3. Distinguishing V-BGS from I-BGS by exposure to H_2O and O_2: (a) BGS of an E-TiO_2 surface are totally healed by 1 L of O_2 at 100 K. (b) BGS of SA-970 K-TiO_2 surface (10 s annealing) are healed at 300 K by H_2O under an electron beam at 38 eV. (c) Same experiment as in (b), but at 22 eV. (d) BGS of SA-470 K-TiO_2 (2100 s annealing) at 300 K are not affected by H_2O under electrons at 38 eV but, in contrast, are healed by O_2. (e) BGS from R-TiO_2 are partially healed at 300 K by H_2O under electrons at 38 eV and even more canceled by further O_2 exposure.

fusion [10,29] from increasingly deeper layers. Assuming that Ti_{int} segregate on step 2 (SA-970 K-TiO_2) over deeper layers than those reached by SA-420 K-TiO_2 (step 3) explains the marginal BGS change on step 3, in an apparent contrast with step 1. The depletion in subsurface Ti_{int} which progressively extends inward [steps 1–4, Fig. 2(c)] suggests that annealing/oxidation cycles can lead to a BGS-free surface region.

The existence of V-BGS has not been singled out yet. Often accepted [16], the attribution to V-BGS of O_b-vac created by electron stimulated desorption (ESD) via the Knotek-Feibelmann process [30,31] is nevertheless strongly discussed [32,33]. Electron bombarded surfaces (E-TiO_2) were prepared by illuminating O-TiO_2 by a 75 eV electron beam (current density $\sim 1\ \mu A\ cm^{-2}$) [30,31]. Totally healed at 100 K by only 1 L O_2 [Fig. 3(a)], the resulting BGS thus stem from very surface defects but, still, there is no indisputable evidence that they are V-BGS. A clue came from the observation that ESD-induced BGS level off at a rather low intensity after 5 min, to remain stable for hours (not shown). Comparisons with other groups show that rather weak BGS were obtained with electron fluxes of $1.25 \times 10^{12}\ e\ cm^{-2}\ s^{-1}$ [34] and $6.25 \times 10^{12}\ e\ cm^{-2}\ s^{-1}$ (this work) while $1.25 \times 10^{15}\ e\ cm^{-2}\ s^{-1}$ [16] and $3 \times 10^{15}\ e\ cm^{-2}\ s^{-1}$ [15] led to strong BGS, although the fluences were similar [$3 \times 10^{15}\ e\ cm^{-2}$ [34]; $2 \times 10^{15}\ e\ cm^{-2}$ (this work); $6–25 \times 10^{15}\ e\ cm^{-2}$ [16]]. Clearly, the electron-induced BGS intensity depends on the flux rather than on the fluence, which suggests a continuous healing of related O_b-vac. We may wonder what is the combined effect of residual water and ESD removal of H adatoms (threshold at 21–22 eV [30,31]). Although reacting O_b-vac by H_2O does not heal BGS [4,35–37], H_2O under 38 eV electrons does heal BGS of SA-970 K-TiO_2 [Fig. 3(b)]. Consistently, 22 eV electrons (threshold for H ESD) have no effect [Fig. 3(c)]. In contrast, I-BGS from SA-420 K-TiO_2 are not healed at 38 eV when exposed to H_2O [Fig. 3(d)], although, as in Fig. 2(d) (step 1), they are healed by O_2. Beyond the demonstration of the existence of V-BGS and I-BGS, the healing of V-BGS via H_2O adsorption provides a means of distinguishing the two states, as in Fig. 3(e), where R-TiO_2 is exposed to H_2O, under a 38 eV electron beam (healing V-BGS) and then exposed to O_2 (healing I-BGS). Notably, the plateau reached by the intensity of the ESD-induced BGS supports their V-BGS nature because, if I-BGS were created, the inability of H_2O to heal them would result in a continuous increase in their intensity.

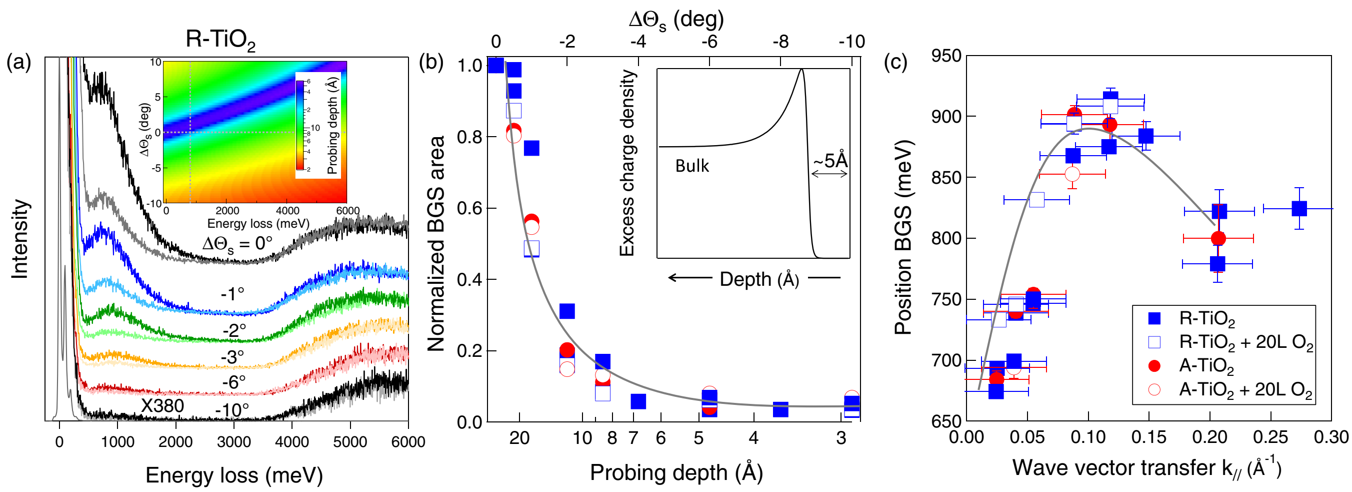

FIG. 4. Concentration profile and dispersion of BGS at 300 K: (a) BGS of R-TiO_2 at different collection angles relative to the specular direction $\Delta\Theta_S = \Theta_S - \Theta_I$ at fixed incidence $\Theta_I = 60^\circ$, as prepared (strong color) and after exposure to 20 L of O_2 (light color). Inset: Calculated off-specular probing depth (see text) averaged over a detector aperture of $\sim 1^\circ$ vs energy loss and angular position $\Delta\Theta_S$ at fixed incident angle at an energy of 38 eV. The gray dotted lines correspond to specular geometry and to BGS energy loss. (b) BGS area normalized to that recorded in specular geometry (maximum probing depth) vs probing depth (bottom scale) and $\Delta\Theta_S$ (top): R-TiO_2 and SA-970 K-TiO_2, as prepared and after 20 L of O_2 at 300 K, are compared. Inset: Schematic concentration profile of excess electrons in the subsurface region. (c) Dispersion of the position of the BGS with the wave-vector transfer $k_\parallel$. $k_\parallel$ error stems from a detector aperture of $\sim 1^\circ$. Gray lines in (b) and (c) are guides for the eye. Color codes for (b) and (c) are given in (c).

Finally, the concentration profiles of the excess electrons and the dispersion of the associated BGS were explored by off-specular EELS (Fig. 4), where the cross section gets more surface sensitive by switching from the dipolar to impact regime [38]. The inverse of the modulus of the wave-vector transfer parallel to the surface gives an estimate of the probing depth [38],

$$k_\parallel = \frac{\sqrt{2mE_I}}{\hbar}\sin\Theta_I - \frac{\sqrt{2m(E_I - \hbar\omega)}}{\hbar}\sin\Theta_S, \qquad (1)$$

where E_I is the incident electron energy, $\hbar\omega$ the energy loss, $2\pi\hbar$ the Planck constant, and Θ_I and Θ_S the incident and scattering angles, respectively (Sec. S3 in Supplemental Material [18]). BGS were recorded off-specular at 300 K, before and after 20 L O_2 exposure, on R-TiO_2 [Fig. 4(a)] and SA-TiO_2 (Fig. S5 in Supplemental Material [18]). Data were normalized to interband transitions whose probing depth does not change significantly with Θ_S [Fig. 4(a) inset and Fig. S2(c) in Supplemental Material [18]]. The dramatic decrease in BGS intensity with Θ_S shows that excess charges are not located at the extreme surface, as confirmed by the poor effect of O_2 at the highest Θ_S. Normalized BGS area versus probing depth from R-TiO_2 and SA-TiO_2 [Fig. 4(b)] and BGS positions versus $k_\parallel$ (Fig. 4(c) show that the four series of data are strikingly similar [Figs. 4(b) and 4(c)]. This shows that the electron localization and state dispersion are independent of whether they are related to O_b-vac (R-TiO_2 and SA-TiO_2) or to Ti_{int} (after O_2 exposure). Generalizing previous theory [39] and experiment [20], the observation directly proves that the surface/subsurface electrostatic potentials dictate the location of the excess charges. A unique representation of the charge distribution can be drawn for all surfaces, either reduced or oxidized [Fig. 4(b) inset]. Going inward, after an almost charge-free atomic layer, excess charges pass through a maximum, consistently with photoelectron diffraction [19,20] and calculations [21–23,37,40]. Going deeper, the defect density lowers to reach the bulk value. The dispersive trend up to a cutoff of $k_\parallel \sim 0.1$ Å^{-1} [Fig. 4(c)] demonstrates the transport behavior of excess electrons down to a distance ($\sim$10 Å) that can be interpreted as the polaron radius at 300 K [22,23,35,37,40,41].

To summarize, vacancy- and interstitial-related BGS have been singled out by EELS experiments based on annealing of the very surface. The associated excess electrons contribute to a unique subsurface distribution whose profile and dispersive behavior are robust with respect to the nature of the defects. In contrast, their role in surface chemistry relies on the specificity of the defects. The dual origin of BGS allows for the understanding of seemingly contradictory observations and opens up different ways of interpreting experiments carried out on TiO_2 surfaces.

J.L. acknowledges support from the China Scholarship Council for his Ph.D. Grant. J.L. did the experimental measurements under the supervision of R.L., with S.C. contributing all the required technical assistance. J.L., R.L., and J.J contributed to interpretations and wrote the manuscript. R.L. and J.J. designed the research strategy.

[1] A. Fujishima, X. Zhang, and D. A. Tryk, Surf. Sci. Rep. **63**, 515 (2008).
[2] M. A. Henderson, Surf. Sci. Rep. **66**, 185 (2011).
[3] U. Diebold, Surf. Sci. Rep. **48**, 53 (2003).

[4] S. Wendt, P. T. Sprunger, E. Lira, G. K. H. Madsen, Z. Li, J. O. Hansen, J. Matthiesen, A. Blekinge-Rasmussen, E. Laegsgaard, B. Hammer *et al.*, Science **320**, 1755 (2008).
[5] Z. Dohnálek, I. Lyubinetsky, and R. Rousseau, Prog. Surf. Sci. **85**, 161 (2010).
[6] C. L. Pang, R. Lindsay, and G. Thornton, Chem. Rev. **113**, 3887 (2013).
[7] V. E. Henrich, G. Dresselhaus, and H. J. Zeiger, Phys. Rev. Lett. **36**, 1335 (1976).
[8] H. Onishi and Y. Iwasawa, Phys. Rev. Lett. **76**, 791 (1996).
[9] M. Li, W. Hebenstreit, L. Gross, U. Diebold, M. A. Henderson, D. R. Jennison, P. A. Schultz, and M. P. Sears, Surf. Sci. **437**, 173 (1999).
[10] E. Lira, J. Hansen, P. Huo, R. Bechstein, P. Galliker, E. Lægsgaard, B. Hammer, S. Wendt, and F. Besenbacher, Surf. Sci. **604**, 1945 (2010).
[11] E. Lira, S. Wendt, P. Huo, J. Ø. Hansen, R. Streber, S. Porsgaard, Y. Wei, R. Bechstein, E. Lægsgaard, and F. Besenbacher, J. Am. Chem. Soc. **133**, 6529 (2011).
[12] E. Lira, P. Huo, J. Ø. Hansen, F. Rieboldt, R. Bechstein, Y. Wei, R. Streber, S. Porsgaard, Z. Li, E. Lægsgaard *et al.*, Catal. Today **182**, 25 (2012).
[13] M. A. Henderson, W. S. Epling, C. L. Perkins, C. H. F. Peden, and U. Diebold, J. Phys. Chem. B **103**, 5328 (1999).
[14] A. C. Papageorgiou, N. S. Beglitis, C. L. Pang, G. Teobaldi, G. Cabailh, Q. Chen, A. J. Fisher, W. A. Hofer, and G. Thornton, Proc. Natl. Acad. Sci. U.S.A. **107**, 2391 (2010).
[15] N. G. Petrik, Z. Zhang, Y. Du, Z. Dohnálek, I. Lyubinetsky, and G. A. Kimmel, J. Phys. Chem. C **113**, 12407 (2009).
[16] C. M. Yim, C. L. Pang, and G. Thornton, Phys. Rev. Lett. **104**, 036806 (2010).
[17] E. Cho, S. Han, H.-S. Ahn, K.-R. Lee, S. K. Kim, and C. S. Hwang, Phys. Rev. B **73**, 193202 (2006).
[18] See Supplemental Material at http://link.aps.org/supplemental/10.1103/PhysRevB.97.041403 for a description of (a) the experimental setup, (b) the annealing of the surface by a hot filament placed in front of the sample, (c) the determination of the probing depth in EELS, and (d) complementary figures.
[19] P. Krüger, S. Bourgeois, B. Domenichini, H. Magnan, D. Chandesris, P. Le Fèvre, A. M. Flank, J. Jupille, L. Floreano, A. Cossaro *et al.*, Phys. Rev. Lett. **100**, 055501 (2008).
[20] P. Krüger, J. Jupille, S. Bourgeois, B. Domenichini, A. Verdini, L. Floreano, and A. Morgante, Phys. Rev. Lett. **108**, 126803 (2012).
[21] S. Chrétien and H. Metiu, J. Phys. Chem. C **115**, 4696 (2011).
[22] N. A. Deskins, R. Rousseau, and M. Dupuis, J. Phys. Chem. C **115**, 7562 (2011).
[23] P. M. Kowalski, M. F. Camellone, N. N. Nair, B. Meyer, and D. Marx, Phys. Rev. Lett. **105**, 146405 (2010).
[24] R. Lazzari, J. Li, and J. Jupille, Rev. Sci. Instrum. **86**, 013906 (2015).
[25] M. A. Henderson, W. S. Epling, C. H. F. Peden, and C. L. Perkins, J. Phys. Chem. B **107**, 534 (2003).
[26] M. A. Henderson, Surf. Sci. **419**, 174 (1999).
[27] Z. Zhang, J. Lee, J. T. Yates, R. Bechstein, E. Lira, J. Hansen, S. Wendt, and F. Besenbacher, J. Phys. Chem. C **114**, 3059 (2010).
[28] K. Mitsuhara, H. Okumura, A. Visikovskiy, M. Takizawa, and Y. Kido, J. Chem. Phys. **136**, 124707 (2012).
[29] S. Wendt, R. Schaub, J. Matthiesen, E. Vestergaard, E. Wahlström, M. Rasmussen, P. Thostrup, L. Molina, E. Lægsgaard, I. Stensgaard *et al.*, Surf. Sci. **598**, 226 (2005).
[30] M. L. Knotek and P. J. Feibelman, Phys. Rev. Lett. **40**, 964 (1978).
[31] J. Lee, Z. Zhang, and J. T. Yates, Phys. Rev. B **79**, 081408 (2009).
[32] S. Wendt, R. Bechstein, S. Porsgaard, E. Lira, J. Ø. Hansen, P. Huo, Z. Li, B. Hammer, and F. Besenbacher, Phys. Rev. Lett. **104**, 259703 (2010).
[33] C. M. Yim, C. L. Pang, and G. Thornton, Phys. Rev. Lett. **104**, 259704 (2010).
[34] K. Onda, B. Li, and H. Petek, Phys. Rev. B **70**, 045415 (2004).
[35] T. Minato, Y. Sainoo, Y. Kim, H. S. Kato, K. Aika, M. Kawai, J. Zhao, H. Petek, T. Huang, W. He *et al.*, J. Chem. Phys. **130**, 124502 (2009).
[36] N. A. Deskins, R. Rousseau, and M. Dupuis, J. Phys. Chem. C **113**, 14583 (2009).
[37] P. G. Moses, A. Janotti, C. Franchini, G. Kresse, and C. G. Van de Walle, J. Appl. Phys. **119**, 181503 (2016).
[38] H. Ibach and D. L. Mills, *Electron Energy Loss Spectroscopy and Surface Vibrations* (Academic, New York, 1982).
[39] T. Albaret, F. Finocchi, C. Noguera, and A. De Vita, Phys. Rev. B **65**, 035402 (2001).
[40] C. M. Yim, M. B. Watkins, M. J. Wolf, C. L. Pang, K. Hermansson, and G. Thornton, Phys. Rev. Lett. **117**, 116402 (2016).
[41] M. Setvin, C. Franchini, X. Hao, M. Schmid, A. Janotti, M. Kaltak, C. G. Van de Walle, G. Kresse, and U. Diebold, Phys. Rev. Lett. **113**, 086402 (2014).